
**Liquid Crystals**
Publication details, including instructions for authors and subscription information:
http://www.informaworld.com/smpp/title~content=t713926090

# X-ray characterisation of local molecular orientation in the electroclinic effect of surface-stabilised SmA liquid crystals

Atsuo Iida[a]; Yumiko Takahashi[b]; Yoichi Takanishi[c]
[a] Institute of Materials Structure Science, High Energy Accelerator Research Organisation, Oho Tsukuba, Ibaraki, Japan [b] Research Institute of Science and Technology, Nihon University, Narashinodai, Funabashi, Japan [c] Department of Physics, Faculty of Science, Kyoto University, Sakyou, Kyoto, Japan

Online publication date: 16 August 2010

**To cite this Article** Iida, Atsuo , Takahashi, Yumiko and Takanishi, Yoichi(2010) 'X-ray characterisation of local molecular orientation in the electroclinic effect of surface-stabilised SmA liquid crystals', Liquid Crystals, 37: 8, 1091 — 1096
**To link to this Article: DOI:** 10.1080/02678292.2010.489155
**URL:** http://dx.doi.org/10.1080/02678292.2010.489155

*Liquid Crystals,*
Vol. 37, No. 8, August 2010, 1091–1096

Taylor & Francis
Taylor & Francis Group

# X-ray characterisation of local molecular orientation in the electroclinic effect of surface-stabilised SmA liquid crystals

Atsuo Iida[a]*, Yumiko Takahashi[b] and Yoichi Takanishi[c]

[a]*Institute of Materials Structure Science, High Energy Accelerator Research Organisation, Oho Tsukuba, Ibaraki, Japan;* [b]*Research Institute of Science and Technology, Nihon University, Narashinodai, Funabashi, Japan;* [c]*Department of Physics, Faculty of Science, Kyoto University, Sakyou, Kyoto, Japan*

(*Received 4 January 2010; final version received 23 April 2010*)

The local molecular orientation in the electroclinic effect of the chiral smectic A phase in a surface-stabilised cell has been determined using a time-resolved synchrotron X-ray microbeam diffraction technique. Space- and time-resolved X-ray wide-angle halo scattering under an electric field reveals the static and dynamic intralayer molecular orientation. The molecular orientation varies spatially in accordance with the stripe texture and is dependent on the applied voltage. It has been found that the deviation of the molecular orientation from the rubbing direction depends strongly on the sample history. The relation between the apparent molecular orientation and the layer structure is discussed.

**Keywords:** electroclinic effect; chiral smectic A phase; surface-stabilised cell; X-ray microbeam; time-resolved technique



## 1. Introduction

Upon application of an electric field in the smectic A (SmA) phase, a tilt in the director of orthogonal SmA liquid crystals is induced near the SmA–SmC* phase transition. This electroclinic effect [1] has been investigated in order to understand the electro-optical behaviour of the pre-transition phenomenon and has been considered to be a potential candidate for electro-optical applications. Analysis of the molecular response within the electroclinic effect has been carried out previously [2–4], and synthesis of novel electroclinic liquid crystals has also been conducted [5, 6]. To understand the electro-optical behaviour in a surface-stabilised cell, it is important to know the dynamics of the layer structure in addition to the molecular orientation. The layer structure of SmA liquid crystals in a surface stabilised cell is known as a bookshelf structure [1]. The shrinkage of the layer spacing due to the molecular tilt of the electroclinic effect produces buckling in the layers of the bookshelf structure, resulting in a horizontal chevron structure. The stripe texture along the layer normal, which can often be observed in the electroclinic effect under a polarising optical microscope, is related to this layer deformation [4, 7–9]. A similar stripe texture also appears in the SmC* and $SmC_A$* phases [8, 9]. This layer structure has been studied both experimentally [10–12] and theoretically [13, 14].

Recently, the static and dynamic local layer structures in the electroclinic effect have been analysed by time-resolved X-ray micro-diffraction using synchrotron X-rays [15]. As the applied field is increased, the layer structure of the electroclinic liquid crystal changes from a bookshelf to a compound chevron structure, and finally to a horizontal chevron structure. During the layer buckling process the surface anchoring in the surface-stabilised cell plays an important role. In order to understand the layer structure, characterisation of the molecular orientation is required. Wide-angle X-ray diffraction is suitable for this purpose because a wide-angle halo pattern offers the information pertaining to the molecular orientation in the layer. However, there has been no report on halo pattern measurement from the local region, possibly due to weak and diffuse halo scattering. In the present study, the time-resolved halo pattern from the local region has for the first time been analysed. The time-resolved molecular orientation as a function of the sample position and the applied voltage is examined and the relationship of the orientation to the layer structure is discussed. Special attention is paid to the process of deformation of the layer structure during prolonged application of an electric field.

## 2. Experimental

The sample and the cell alignment condition were as in previous experiments [15, 16]. A ferroelectric liquid crystal sample (TK–C101 (Chisso)) [15] was sandwiched between indium tin oxide (ITO)-coated glass plates (80 μm thick), with polyimide alignment films. The phase sequence of TK–C101 is isotropic (80°C) N* (70°C) SmA (56°C) SmC*. The experiments were performed in the SmA phase at 0.5°C to 1.0°C

*Corresponding author. Email: atsuo.iida@kek.jp

ISSN 0267-8292 print/ISSN 1366-5855 online

DOI: 10.1080/02678292.2010.489155
http://www.informaworld.com

above the phase transition temperature. The experiments were carried out with one-sided rubbing cells. The cell gap was about 7 μm.

The X-ray experimental conditions are briefly described as follows (further details are given in [16]). The synchrotron X-ray diffraction experiments were carried out on beam-line 4A at the Photon Factory (Tsukuba, Japan). The incident X-ray energy was 14.2 keV (0.873 Å) for measurement of the halo pattern. The incident beam size was approximately 3(h) × 4(v) $\mu m^2$ and the angular divergence of the beam was about 3.0 mrad in both horizontal and vertical directions. The incident X-ray intensity was adjusted to keep the layer diffraction intensity constant during the experiment, in order to minimise radiation damage. The X-rays were incident on the sample normal to the cell surface. The rubbing direction was set to be horizontal.

The halo patterns were recorded using an image-intensified CCD X-ray camera (Hamamatsu C4880–50) with a 133 × 133 mm field of view. For measurement of the halo pattern with the X-ray microbeam, careful reduction of the background is crucial because of the weak and diffuse scattering intensity.

Furthermore, it is not possible to use strong incident X-rays due to radiation damage to the liquid crystal sample. To give the required statistical accuracy, data for the diffuse halo pattern were collected up to the saturation level of the detector (a well depth of 16 bits) for each measurement cycle and then summed. The effective exposure time to obtain the halo pattern at a given point was around 300 s. Figure 1(a) shows the typical halo pattern obtained from the sample in the cell under the electric field.

The background intensity, obtained from the cell without the liquid crystal, was subtracted from the raw data. The inner circular region of low intensity was due to the presence of an attenuator, with a small central lead direct beam stop, for the suppression of the strong forward scattering intensity, in addition to the first-order layer diffraction, which appears in the horizontal direction. The outer rings are caused by X-ray diffraction from the crystalline ITO thin films. The halo pattern, which consists of two short diffuse arcs appearing on the upper and lower sides in the vertical direction, is due to the molecular arrangement of the smectic layer. The absolute value of the average scattering vector of the halo pattern is around 29 $nm^{-1}$, which makes the average intralayer molecular distance around 0.43 nm.

In order to obtain quantitative information about the halo pattern, the angular intensity distribution integrated over the certain ring width was extracted, as shown in Figure 1(b). The angle zero is along the horizontal direction, indicated by an arrow in Figure 1(a), and the angle is measured anticlockwise. Using a curve-fitting procedure, the angular position and width of the diffuse halo peak were established. The average molecular orientation is considered to be normal to the angular peak position. Although the full width at half maxima of the halo pattern angular distribution was also evaluated, its dependence on the position and the applied field could not be assessed quantitatively due to the insufficient statistics obtained.

The spatial variation in the molecular orientation of the electroclinic effect, together with the response to the polarity change of the applied field, were measured

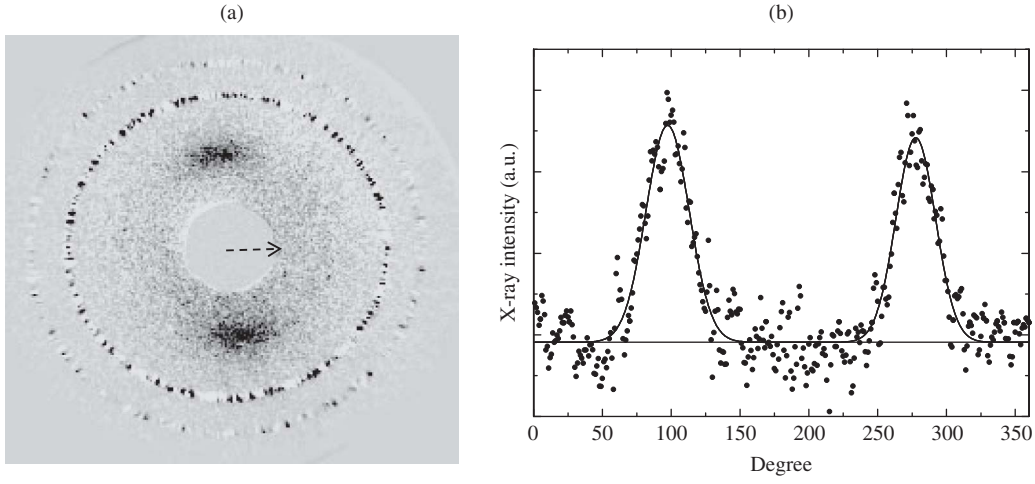


Figure 1. (a) Two-dimensional X-ray diffraction pattern obtained from a SmA liquid crystal after background subtraction. The outer granular rings are diffraction peaks from a crystalline ITO thin film; (b) angular intensity distribution of the halo pattern extracted from (a). The angle is measured anticlockwise from zero, indicated by an arrow in (a).

under the square waveform electric field (5 Hz, ±13 V) using a time-resolved technique, in which the diffraction data under a positive or negative applied field were stored separately. The molecular response to the triangular waveform was also measured in the time-resolved mode in order to measure the voltage dependence of the molecular orientation.

## 3. Results

After application of the square electric field, the sample exhibited a stripe texture under the polarising optical microscope, shown in Figure 2(a).

Figure 3(a) shows the angular position of the halo peak as a function of the Y direction, i.e. across the stripe pattern, during the square field application. The peak angular position varies with a spatial period of around 10 μm, and its amplitude ($2\alpha'$) is around 3°. This spatial periodicity is approximately the same as the width of the stripe texture in Figure 2(a). The shift of the peak angular position between the positive and negative applied fields, measured using the time-resolved mode ($2\theta'$), is about 6°.

Two days later the same cell sample was again measured, and the results are presented in Figure 3(b). During those two days, the sample temperature was

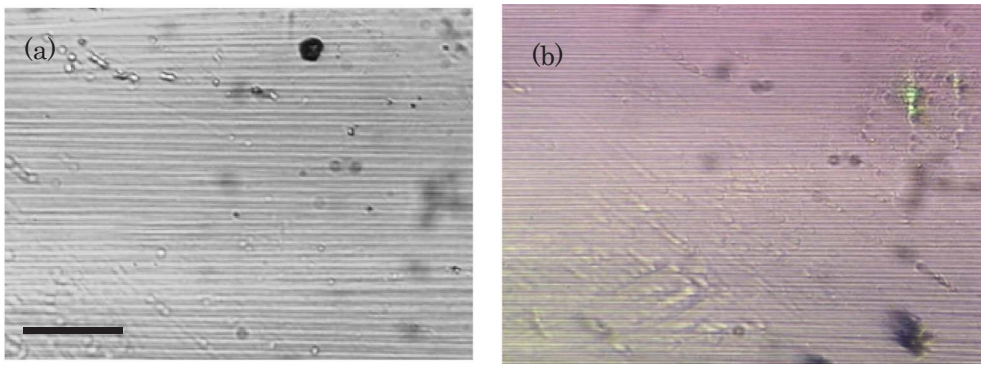


Figure 2. Polarised optical micrographs of textures after square wave field application as a function of time; (b) four days later than (a). The scale represents a distance of 100 μm (colour version online).

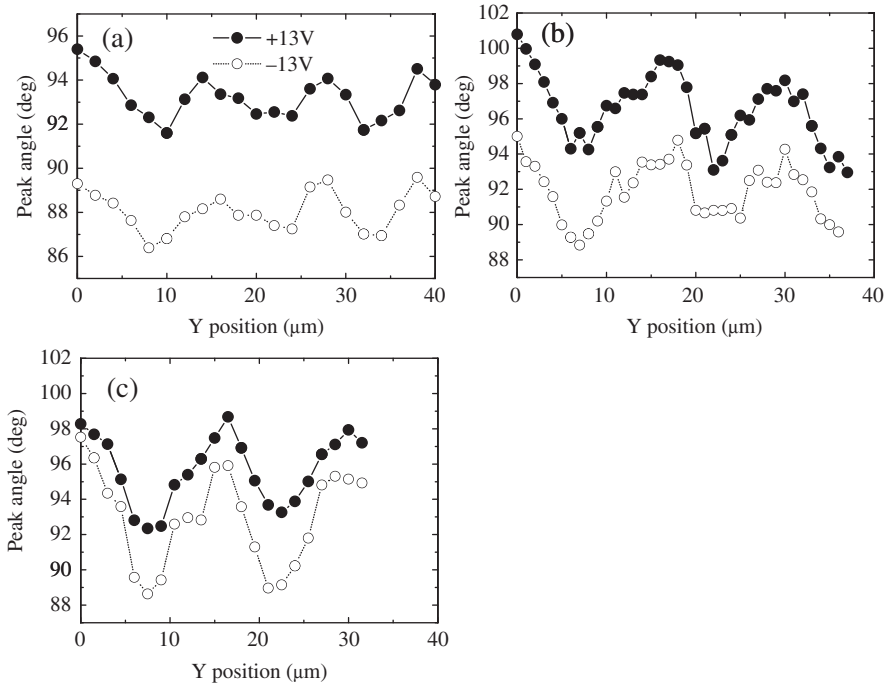


Figure 3. Halo peak angular positions as a function of vertical sample position (*Y*-axis). (a), (b) and (c) were obtained at the same position, while each of the graphs was obtained after an interval of two days. Closed and open circles correspond to positive (+13 V) and negative (–13 V) applied fields, respectively.

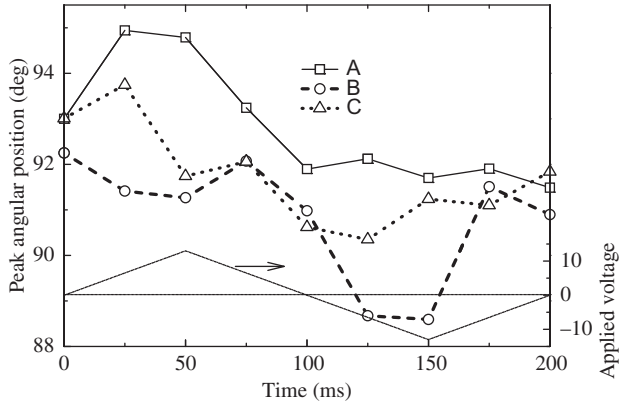


Figure 4. Peak angular position of the halo pattern as a function of time for a triangular electric waveform. The three curves, A, B and C, were obtained at different positions that were 4 μm apart. The right-hand vertical axis represents the applied triangular electric field (5 Hz, ±13 V).

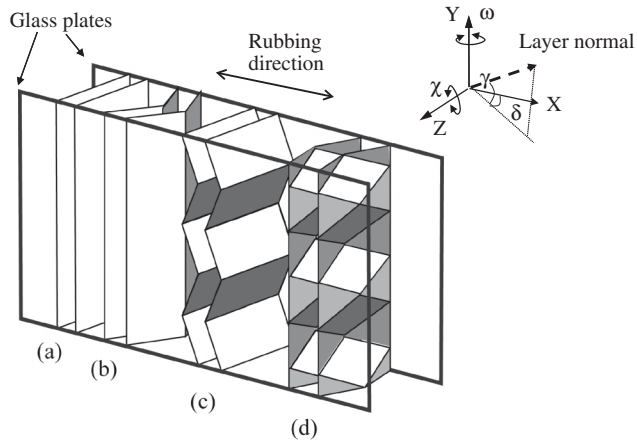


Figure 5. Schematic drawing of layer structures of smectic liquid crystals: (a) bookshelf, (b) vertical chevron, (c) horizontal chevron and (d) compound chevron (vertical and horizontal structure). Coordinates and rotation axes are shown. X-rays are incident along the $Z$-axis. $\delta$ and $\gamma$ are the layer deflection angles.

kept constant, while the applied waveform was changed, with a maximum applied voltage of less than ±13 V. The amplitude of the peak angular position ($2\alpha'$) is around 6°, an increase from 3° in Figure 3(a). The shift in peak position due to the reversal in the polarity of the applied field ($2\theta'$) is around 6°. The spatial periodicity was slightly longer than 10 μm.

After a further two days the amplitude of the peak angular position ($2\alpha'$) increases slightly to around 7° and the peak position shift due to the polarity reversal ($2\theta'$) is 3° to 4° (Figure 3(c)). It is also noted that the contrast in the stripe texture shown in Figure 2(b) is weaker than that in Figure 2(a).

In order to clarify the dependence of the halo pattern on the applied voltage, the time-resolved measurements (time resolution 25 ms) under the triangular waveform (5 Hz, ±13 V) were carried out as shown in Figure 4, and were obtained just after the square wave measurement in Figure 3(b). The time-resolved (voltage-dependent) peak angular positions were obtained from three separate positions at 4 μm intervals along the $Y$ direction. The peak angular positions of curves A and B move in the opposite direction in the first (positive field) and second (negative field) half of the applied triangular field, respectively, while curve C lies in between.

## 4. Discussion

The rotation of the halo pattern reflects the molecular motion in the electroclinic effect, in which the molecules tilt with respect to the layer normal in response to the applied electric field, resulting in layer shrinkage. To accommodate this shrinkage the layer transforms locally into a horizontal chevron structure (the layer rotation around the cell surface normal as shown in Figure 5(c)). The process by which the horizontal chevron is formed is similar to that for the vertical chevron in the SmC* phase, when the liquid crystal is cooled from the SmA* phase (Figure 5(b)) . The formation of the horizontal chevron and its response to an electric field have previously been discussed based on X-ray measurements [11, 17–20] and are shown schematically in Figure 6(a). The layer bends in alternate directions at angle α, generating a stripe texture parallel to the layer normal; the molecules in one stripe (region **a** in the central panel in Figure 6(a)) slide along the rubbing direction, while those in the neighbouring stripe (region **b**) rotate $2\theta$ (where $\theta$ is the tilt angle) from the initial direction. When the polarity of the applied field is reversed the molecule tilts in the opposite direction, as shown in the right-hand panel. The expected spatial variation in the angular position of the halo peak (the molecular tilt) is shown in Figure 6(b). For the triangular field application, the molecules in stripe **a** remain parallel to the rubbing direction, independent of the applied voltage, whereas those in the neighbouring stripe **b** rotate as a function of the applied voltage, as shown in the first half of Figure 6(c). When the sign of the applied field is reversed (second half of Figure (6c)), the molecules in stripe **a** rotate, whereas those in stripe **b** do not. Figures 6(b) and (c) are drawn for $\alpha = \theta$.

In the current series of measurements of the peak angular position of the halo scattering across the stripe, the results in Figure 3(b) correspond to the molecular motion shown in Figure 6(b) ($\alpha \approx \theta \approx 3°$).

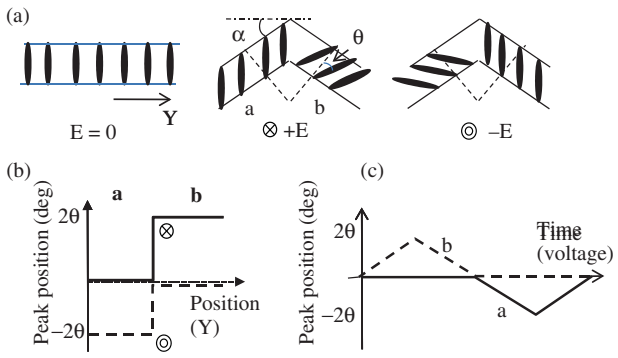


Figure 6. Schematic representation of the molecular and layer response of electroclinic liquid crystals under an electric field (a) with molecule tilt angle, $\theta$, and layer deflection angle, $\alpha$; (b) the peak angular position of the halo pattern for the square electric field as a function of the vertical sample position for positive (solid line) and negative (dotted line) electric field; and (c) that for the triangular electric field at adjacent stripe regions as a function of time (voltage). Figures are drawn for $\alpha = \theta$. **a** and **b** indicate the two adjacent stripe regions shown in (a). The zero of the peak position is normal to the initial bookshelf layer.

In this case, the amplitude of the spatial dependence of the halo peak angular position ($\alpha'$), and the halo peak angular position difference for the applied field polarity reversal ($\theta'$), correspond to $\alpha$ and $\theta$, respectively. The applied voltage dependence, i.e. the time-resolved measurement under the triangular wave form shown in Figure 4, can be explained by Figure 6(c). The local molecular orientation variation and the time-resolved orientation response shown in Figure 6 are thus for the first time confirmed experimentally.

The halo peak angular position, however, depends strongly on the sample history. At the initial stage of application of the field, the angle $\alpha'$ in Figure 3(a) is smaller than that in Figure 3(b), whereas angle $\theta'$ is nearly the same. At a later stage, the angle $\alpha'$ in Figure 3(c) is almost the same as that in Figure 3(b), while $\theta'$ becomes smaller. In our previous paper [15], we reported that the layer structure transforms reversibly between the bookshelf (low field strength, Figure 5(a)) and the compound chevron (medium field, Figure 5(d)) at the medium applied field. At high field the horizontal chevron becomes the dominant structure. A compound chevron structure is created because it is difficult for the molecule near the interface (the alignment film) to move from the alignment direction at the initial stage of the electric field application. In order to minimise the deviation angle of the molecule from the rubbing direction a small layer deflection angle is preferable, although global d-spacing adjustment is needed. At this stage, when $\alpha < \theta$ the maximum deviation angle, $\alpha + \theta$, is less than $2\theta$, resulting in $\alpha' < \theta'$.

After prolonged application of the field (Figure 3(b)), the molecules responds to the field, as explained in Figure 6(a), and the maximum deviation angle increases to $2\theta$. At this stage, the layer structure has assumed a mostly horizontal chevron structure.

In the later stages of the field application the horizontal chevron structure was well developed, even after the applied field was turned off [16], in other words the molecules were not parallel to the rubbing direction even when the electric field was turned off. The deflection angle, $\alpha$, may be larger than the molecular tilt angle ($\theta$), and the maximum deviation angle, $\alpha + \theta$, is larger than $2\theta$, resulting in $\alpha' < \theta'$.

Although information about the layer structure, in addition to molecular orientation can be obtained from the halo pattern, the simultaneous measurement of the layer structure (small angle) and the molecular orientation (wide angle) must be performed with higher precision in order to fully understand the dynamics of the electroclinic effect. Furthermore, since the molecular reorientation due to the electroclinic effect causes layer spacing shrinkage, precise measurement of the layer spacing might be an effective approach. Techniques to improve these areas are being developed.

In summary, the molecular orientation of the electroclinic effect in the SmA liquid crystal in a cell has been studied in terms of the halo pattern, using a time-resolved synchrotron X-ray microbeam for the first time, and the dynamics of molecular orientation and the layer structure have been discussed.

## Acknowledgements

The authors wish to thank the staff of the Photon Factory for their help during the experiments. The authors are also grateful for valuable discussions with Professor H. Takezoe, and to Ms Y. Ohtsuka for her help with the experiments.

This study was carried out under the approval of the Photon Factory Advisory Committee (Proposals 06G345 and 08G697). It was partially supported by Grant-In-Aid for Scientific Research (B) (18360013), the Ministry of Education, Science, Sports and Culture.

## References

[1] Garoff, S.; Meyer, R.B. *Phys. Rev. Lett.* **1977**, *38*, 848–851.
[2] Lagerwall, S.T. *Ferroelectric and Antiferroelectric Liquid Crystals*; Wiley: Weinheim, 1999.
[3] Williams, P.A.; Clark, N.A.; Ros, M.B.; Walba, D.M.; Wand, M.D. *Ferroelectrics* **1991**, *121*, 143–146.
[4] Pavel, J.; Glogarova, M. *Liq. Cryst.* **1991**, *9*, 87–93.
[5] Clark, N.A.; Bellini, T.; Shao, R.-F.; Coleman, D.; Bardon, S.; Link, D.R.; Maclennan, J.E.; Chen, X.-H.; Wand, M.D.; Walba, D.M.; Rudquist, P.; Lagerwall, S.T. *Appl. Phys. Lett.* **2002**, *80*, 4097–4099.

[6] Hayashi, N.; Kato, T.; Fukuda, A.; Vij, J.K.; Panarin, Y.P.; Naciri, J.; Shashidhar, R.; Kawada, S.; Kondoh, S. *Phys. Rev. E: Stat., Nonlinear, Soft Matter Phys.* **2005**, *71*, 041705-1-8.
[7] Shao, R.F.; Williams, P.C.; Clark, N.A. *Ferroelectrics* **1991**, *121*, 127–136.
[8] Johno, M.; Ouchi, Y.; Takezoe, H.; Fukuda, A.; Terashima, K.; Furukawa, K. *Jpn. J. Appl. Phys.* **1990**, *29*, L111–L114.
[9] Fünfschilling, J.; Schadt, M. *Jpn. J. Appl. Phys.* **1991**, *30*, 741–746.
[10] Rieker, T.P.; Clark, N.A.; Smith, G.S.S.; Parmar, D.S.; Sirota, E.B.; Safinya, C.R. *Phys. Rev. Lett.* **1987**, *59*, 2658–2661.
[11] Geer, R.E.; Singer, S.J.; Selinger, J.V.; Ratna, B.R.; Shashidhar, R. *Phys. Rev. E: Stat., Nonlinear, Soft Matter Phys.* **1998**, *57*, 3059–3062.
[12] Williams, P.A.; Clark, N.A.; Ros, M.B.; Walba, D.M.; Wand, M.D. *Ferroelectrics* **1991**, *121*, 143–146.
[13] Selinger, J.V.; Xu, J.; Selinger, R.L.B.; Ratna, B.R.; Shashidhar, R. *Phys. Rev. E: Stat., Nonlinear, Soft Matter Phys.* **2000**, *62*, 666–674.
[14] Tang, Anlun; Sprunt, S. *Phys. Rev. E: Stat., Nonlinear, Soft Matter Phys.* **1998**, *57*, 3050–3058.
[15] Iida, A.; Takahashi, Y.; Takanishi, Y.; Nakata, M.; Ishikawa, K.; Takezoe, H. *Liq. Cryst.* **2005**, *32*, 717–726.
[16] Takahashi, Y.; Iida, A.; Takanishi, Y.; Ogasawara, T.; Nakata, M.; Ishikawa, K.; Takezoe, H. *Phys. Rev. E: Stat., Nonlinear, Soft Matter Phys.* **2003**, *67*, 051706-1-10.
[17] Crawford, G.P.; Geer, R.E.; Naciri, J.; Shashidhar, R.; Ratna, B.R. *Appl. Phys. Lett.* **1994**, *65*, 2937–2939.
[18] Rappaport, A.G.; Williams, P.A.; Thomas, B.N.; Clark, N.A.; Ros, M.B.; Walba, D.M. *Appl. Phys. Lett.* **1995**, *67*, 362–364.
[19] Rindle, J.R.; Bartoli, F.J.; Flom, S.R.; Harter, A.T.; Ratna, B.R.; Shashidhar, R. *Appl. Phys. Lett.* **1997**, *70*, 1536–1538.
[20] Dirking, I.; Glusen, B.; Lagerwall, S.T.; Ober, C.K. *Phys. Rev. E: Stat., Nonlinear, Soft Matter Phys.* **2000**, *61*, 1593–1598.